

Microstructure and mechanical property characterisation of aluminium–steel joints fabricated using ultrasonic additive manufacturing*

Niyanth Sridharan^{a,b}, Paul Wolcott^c, Marcelo Dapino^c and Sudarsanam Suresh Babu ^{a,b}

^aDepartment of Mechanical, Aerospace, and Biomedical Engineering, University of Tennessee, Knoxville, TN, USA; ^bManufacturing Demonstration Facility, Oak Ridge National Laboratory, Oak Ridge, TN, USA; ^cDepartment of Mechanical and Aerospace Engineering, The Ohio State University, Columbus, OH, USA

ABSTRACT

Driven by the interest to weld steel and aluminium (Al) in the solid state to prevent intermetallic formation, 9 kW ultrasonic additive manufacturing (UAM) has been used to fabricate Al 6061–4130 steel dissimilar metal builds. In addition, Al 6061–6061 builds were fabricated using similar techniques to provide a baseline for mechanical property measurement. Mechanical testing performed using pushpin testing shows that steel–Al dissimilar metal welds fail across multiple layers while Al–Al welds delaminate from the substrate. Multi-scale characterisation indicates that the change in failure morphology is due to the formation of metallurgical bonds in the Al–steel builds. Texture analysis shows identical textures at the interface of Al–steel, Al–Al and Al–Ti joints; showing that the bond formation in all cases relies extensively on plastic deformation across multiple materials. In addition, no changes to the bonding mechanism occurred when the materials used as foils and substrate were swapped.

ARTICLE HISTORY

Received 3 September 2016
Accepted 9 October 2016

KEYWORDS

Ultrasonic additive manufacturing; Al–steel; dissimilar metal welding; microstructure characterisation

Introduction

There is an increased drive towards light weighting of materials for enhancing energy efficiency in both the automotive and aerospace industries. To fabricate such lightweight structures, dissimilar metal joining is necessary to enable integration of multiple subsystems. Of specific interest, aluminium (Al) and steel combinations are widely used in the automotive and the aerospace sector to effect light weighting of parts [1].

While resistance spot-welding is widely adopted for joining Al to steel in the automotive industry, frequent electrode wear and tool replacement limit its use in Al and steel dissimilar joints [1]. Liquid metal embrittlement during resistance spot welding can also degrade the mechanical strength of these joints. Similarly, various intermetallic phases can form during fusion welding of Al and steel, resulting in brittle failures at these interfaces [2].

To avoid intermetallics and liquid metal embrittlement, friction stir welding, a solid state welding process, has been widely used to fabricate dissimilar metals. However its use to fabricate Al–steel joints is challenging due to the difference in deformation and physical properties of Al and steel [3]. This discontinuity in properties across the abutting surfaces will have significant influence on the stirring properties of the materials [4]. Hence, materials for the advancing and the

retreating side need to be selected carefully to obtain optimum mixing and therefore control the mechanical properties [4]. For instance, an increase in the amount of martensite can be obtained by orienting the steel in the advancing side of the tool [5]. Selection of process parameters is critical to control the extent of intermetallic formation at the interface [6]. It has been reported that the mechanical properties of these welds are a function of the intermetallic thickness. Welds with intermetallic thickness less than 5 µm do not show a deterioration in properties while when the intermetallic thicknesses exceed 5 µm a sharp decrease in the mechanical strengths are observed [6,7].

There are several other high strain rate processes such as magnetic pulse welding and magnetic seam welding where it is claimed that there is no interfacial reaction during welding. Literature suggests that the intermetallic formation during high strain rate welding is a function of process parameters [8,9]. Increases in impact velocity tend to increase the possibility of intermetallic formation due to localised melting [10]. Hence solid-state welding techniques that involve no macroscopic rise in temperature are necessary to fabricate welds to avoid intermetallic formation.

Additional solid-state welding techniques, such as ultrasonic welding, can facilitate dissimilar welding without intermetallic formation. Ultrasonic additive

CONTACT Niyanth Sridharan  niyanth.sridharan@gmail.com  Department of Mechanical, Aerospace, and Biomedical Engineering, University of Tennessee, 1512 Middle Drive, 414 Dougherty, Knoxville, TN37996-2210, USA

This manuscript has been authored by UT-Battelle, LLC, under Contract No. DE-AC05-00OR22725 with the U.S. Department of Energy. The United States Government retains and the publisher, by accepting the article for publication, acknowledges that the United States Government retains a non-exclusive, paid-up, irrevocable, worldwide license to publish or reproduce the published form of this manuscript, or allow others to do so, for United States Government purposes. The Department of Energy will provide public access to these results of federally sponsored research in accordance with the DOE Public Access Plan (<http://energy.gov/downloads/doe-public-access-plan>).

manufacturing is a technique which couples ultrasonic welding, mechanised tape layering and CNC machining to fabricate complex shapes [11,12]. It shows promise in the creation of layered metallic structures, with similar and dissimilar material combinations. The macroscopic temperature rise at the interface has been measured to be less than 200°C for welding Al [13]. However, the actual temperature that the interface experiences due to adiabatic heating effects from severe plastic deformation is debated in the literature [14].

The feasibility of using UAM to fabricate dissimilar metal welds has been shown [15,16]. Truog [17] investigated the effect of post-weld heat treatment of Al–Cu UAM builds and observed an increase in the bond strengths after post-weld heat treatment. Post-weld characterisation showed the formation of a thin layer of intermetallic at the interface which provides a constraint during deformation resulting in a more energetic failure of the builds [17]. The effect of increased surface roughness of the tapes also enhanced energy to failure and the reason was attributed to increased mechanical interlocks between the dissimilar metals. Previous work has shown that while welding dissimilar metal combinations such as Al–1100 and CP titanium, the deformation is primarily concentrated in the softer metal while the harder Ti does not deform [18,19]. While the welding of metal combinations such as Al–Al [11,12,20,21], Al–Cu [17], and Al–Ti [15,16,18,19] has been well studied, there are currently limited studies which address the challenges of welding steels using this technique.

Limited feasibility studies have been performed on Al–steel using ultrasonic spot welding. Prangnell et al. [1] show that while it is possible to fabricate Al–steel joints, the process involves using three times more power than is needed to fabricate Al–Al welds [1]. They also show that the intermetallic formation tendency depends primarily on the time of welding, where the intermetallic formation occurred only when the weld time exceeded 1.5 s where a larger weld time corresponds to a larger input power [1]. The application of weld power in UAM is controlled by the normal force, vibration amplitude and travel speed of the sonotrode [20,21]. Under higher weld power, the material is subjected to increased plastic deformation, which is necessary for weld strength [22]. The strength levels of solid state welds increase with deformation and reach a plateau, governed by the strength of the weaker metal [23].

As stated above only the softer metal undergoes deformation during welding a hard and a soft metal combination. Owing to this difference in deformation characteristics, it is not known if this would contribute to the formation of a solid-state bond since both the materials need to co-deform. Hence the aim of this work is to

- (i) Explore the feasibility of joining 4130 steel and Al–6061 using UAM.
- (ii) Compare the bond strength of dissimilar Al 6061–4130 steel to that of the similar Al 6061–6061 welds.
- (iii) Multi-scale characterisation to determine if a metallurgical bond can form in Al–steel and compare the mechanism of bonding with other dissimilar metal combinations.

Experimental procedure

Sample manufacturing

Joining of Al–steel combinations was investigated using a 9 kW UAM machine at The Ohio State University. Combinations of Al (tape will be referred to as ‘T’) onto steel (substrate will be referred to as ‘S’) and steel (T) onto Al (S) were investigated. In each case, the substrate used was machined flat prior to welding to remove oxide scales from the surface and ensure flatness. Welds onto steel utilised an annealed 4130 baseplate, while welds onto Al were joined using a 6061–T6 baseplate. For each case, the first foil layer in contact with the baseplate constituted a dissimilar weld. Subsequent welds, for the case of Al onto steel were similar Al–Al joints. The weld parameters for the Al (T) onto steel (S) joining were 5000 N normal force, 23 μm weld amplitude, and a welding speed of 100 in. min^{-1} , all conducted on a substrate preheated to 300°F. The similar Al–Al bonds were performed using a 5000 N normal force, 32.5 μm weld amplitude and 200 in. min^{-1} (84.66 mm s^{-1}) weld speed. The Al (T)–Al (T) bonds were fabricated using optimised process parameters from previous studies [24]. For the case of steel (T) onto Al (S), the process parameters used for these welds were 5000 N weld force, 41.6 μm amplitude, 100 in. min^{-1} weld speed and a baseplate temperature of 300°F.

Joint characterisation

After fabrication, mechanical testing of the joints was performed on the Al (T)–steel (S) builds using pushpin testing. Pushpin testing is a testing method introduced by Zhang et al. to evaluate the mechanical performance of the laminated structures [25]. The advantage of pushpin testing over other tests such as a peel test is due to the fact that the failure always occurs within the weld, thus providing a measure of weld strength. Peel tests, for example, can fail in the foil material itself, therefore limiting the information gained from the test [26]. Pushpin tests were performed on 10 layer samples using a Gleeble 3800 thermo-mechanical test frame at room temperature. During the test, a pin is pressed through the sample at 0.2 mm s^{-1} with the load and displacement being recorded. The maximum force of the push out as well as the area under the

curve, are the two metrics used to analyse the results of the test. More information on the test can be found elsewhere [25].

After mechanical testing multi-scale characterisation was performed to rationalise the differences in mechanical strengths. Analysis was performed using scanning electron microscopy (SEM), electron backscattered diffraction (EBSD) and transmission electron microscopy (TEM) to investigate the effects of the processing. To facilitate the microstructural analysis, samples were sectioned using a low speed diamond saw and cold mounted in epoxy to prevent any changes to the dislocation substructure introduced during the UAM process. The samples were polished using standard metallography techniques. SEM and EBSD were performed on a JEOL 6500S electron microscope with an accelerating voltage of 20 kV and a probe current of 4 nA. Samples for analysis on the TEM were prepared using focused ion beam machining. Transmission electron microscopy was performed using the JEOL 2100 (S)TEM at an accelerating voltage of 200 KeV.

Results and discussions

Mechanical testing of the interfaces

Pushpin testing was performed on the samples to evaluate the bond strength of the Al (T) foils on the steel (S) configuration. Testing was performed only on this configuration due to difficulties joining steel (T)-to-steel (T) joints to reach the necessary sample dimensions. Three tests were performed on the dissimilar builds and compared to the results obtained from similar tests from Al–Al builds fabricated using optimised parameters. Results of the pushpin tests for each of the material combinations can be found in Figure 1(a) and (b). The Al–steel builds exhibited an average maximum load of 2.85 kN, and an area under the curve, or integral, of 5.15 kN-mm. Al–Al builds resulted in an average maximum push out force of 1.67 kN and an integral of 1.53 kN-mm. The force–displacement

curves are shown in Figure 1(a) and (b) for each of the material combinations tested. As shown, despite the failure modes being very similar in $\sim 80\%$ of the sample (i.e. delamination) the Al–steel combinations produce significantly higher mechanical strength than the Al–Al similar metal combination.

A region at the edge of the build (marked in Figure 2(a)) did not delaminate during failure. The plausible reasons why the region did not delaminate could be attributed to mechanical interlocks, higher strengths due to the enhanced plastic deformation, metallurgical bonds or a combination of all the three.

Multiscale characterisation was performed on the bonded regions on the area marked in Figure 2(a) to understand the reason for the enhanced strengths of the Al–steel interfaces.

Microstructure characterisation

Optical microscopy shown in Figure 2(a) and (b) did not reveal any typical defects previously observed and reported [27], indicating successful bonding occurred. One plausible hypothesis for the enhanced strength of the un-failed interface is the deformation concentrated in the interface of the softer Al resulting in excessive deformation due to the larger power input into the weld. Normally the strength levels of solid state welds increase with deformation and reach a plateau [23]. To further understand, the effects of plastic deformation at the interface, EBSD was performed on the Al–steel and Al 6061–6061 interfaces. The results are shown in Figure 3(a) and (c). The dark region seen at the interface in 3(a) is a consequence of shadowing arising from dissimilar polishing in the Al and steel regions. Figure 3(b) and (c) shows the Al–steel and the Al–Al interfaces at higher magnification indicating the refinement of the grains at the interface.

In the Al–6061 foils deposited on the steel plate, the deformation is localised only on the Al interfaces. This is based on the observation of grain refinement only on the Al side of the interface shown in Figure 3(a)

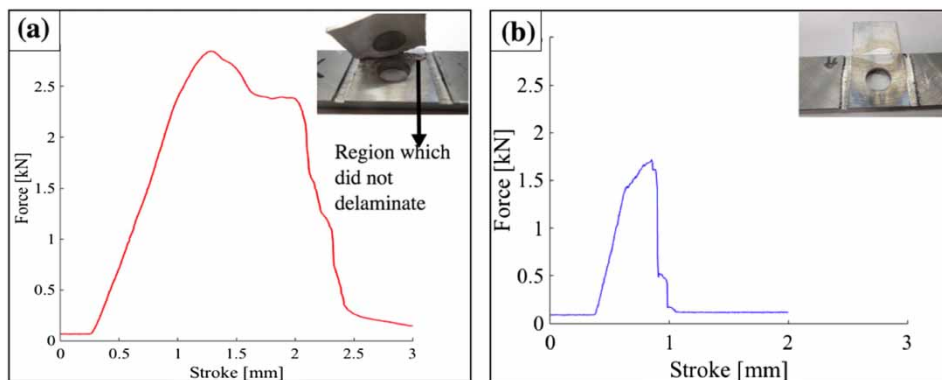


Figure 1. Load–stroke curve of the pushpin tests (a) Al 6061–4130 steel dissimilar metal weld (b) Al 6061–6061 weld. Note the difference in the failure morphology in both the similar and dissimilar welds shown in the fracture photographs.

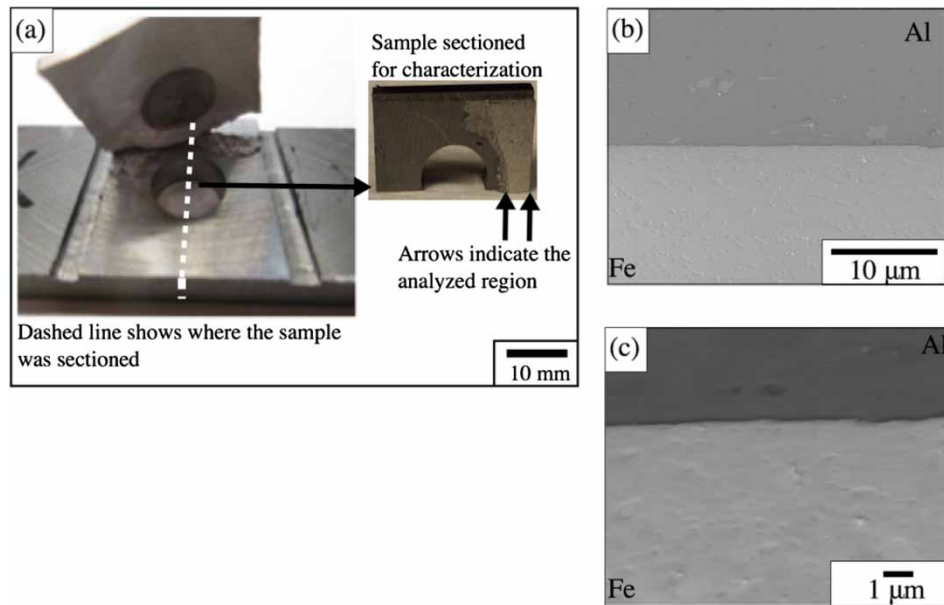


Figure 2. (a) Figure shows the locations where microstructure analysis was performed; (b) Al–steel interface showing the absence of defects; (c) Al–steel interface at higher magnification. (b) and (c) The absence of any voids or defects at the interface.

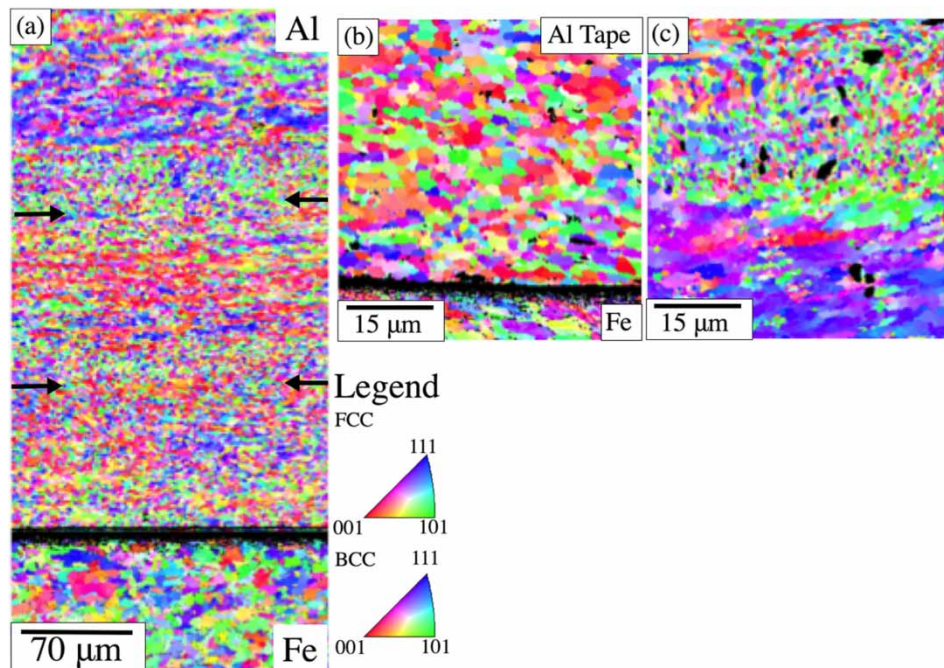


Figure 3. (a) Inverse pole figure of the Al–steel dissimilar metal weld. The Al–Al similar interfaces are marked with black arrows. The dark region at the steel–Al interface arises due to the shadowing effect of electrons; (b) Al–steel interface at higher magnification showing extensive grain refinement; (c) Al–Al interface at higher magnification showing similar refinement of the grains.

and (b). This is expected to be due to the high hardness differences between the Al (87.3 HVN) and steel (150 HVN). On examining the backscatter diffraction obtained from the Al–Al interface, it is clear that the Al–Al interfaces also show similar features indicating that enhanced plastic deformation in the dissimilar metal combination is not the reason for the observed failure behaviour. The observed grain refinement at the interfaces could be promoted by two mechanisms,

continuous dynamic recrystallisation (cDRX) and discontinuous dynamic recrystallisation (dDRX) and has been discussed elsewhere in some detail [13,18,28,29].

The only possibility of the Al–steel weld showing higher strengths is if the interface marked in Figure 2(a) shows metallurgical bonding. Two conditions are necessary for metallurgical bonding to occur namely (i) Oxide removal; (ii) asperity collapse [23,30].

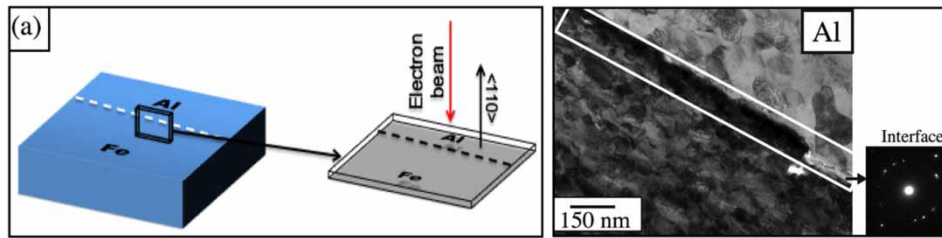


Figure 4. (a) Schematic of sample extraction for the TEM analysis and the orientation of the sample with respect to the electron beam; (b) the TEM micrograph of the interface. The selected area diffraction pattern at the interface show diffraction rings indicating the presence of a nano-crystalline region at the interface.

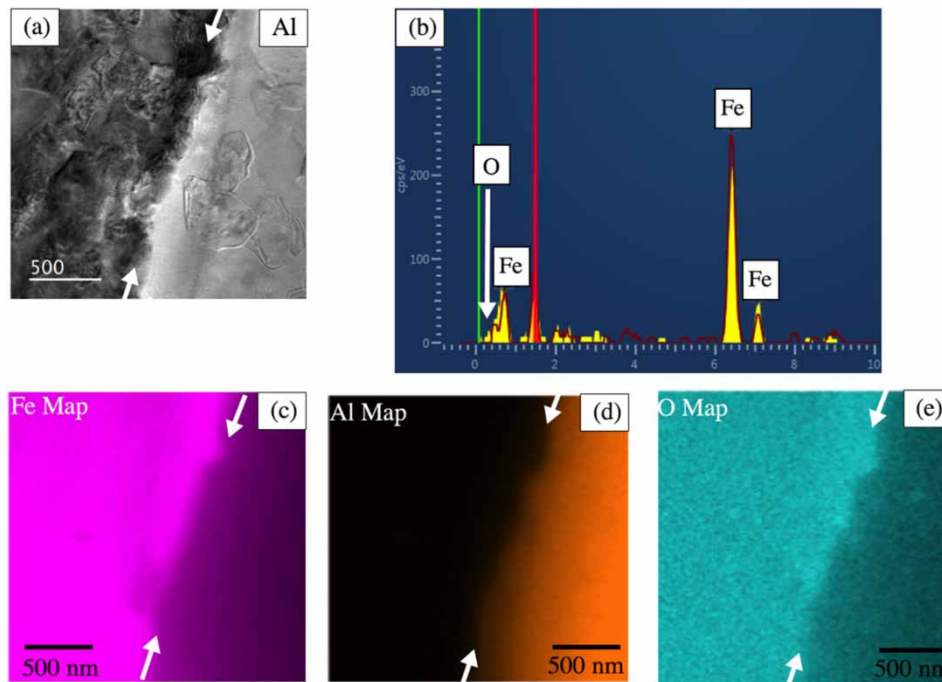


Figure 5. (a) HAADF-STEM image of the interface showing mottled contrast at the interface (marked using white arrows). (b) EDS spectrum of the spot analysis performed at the interface showing the absence of any oxygen peaks at the interface. (c)–(e) shows the elemental maps of the (c) Fe, (d) Al and (e) oxygen.

Figures 2–4 show the presence of plastic deformation that resulted in the collapse of asperities. To investigate the effectiveness of oxide removal, transmission electron microscopy in conjunction with energy dispersive spectroscopy was performed.

The results from TEM investigations are shown in Figure 4. As shown in the EBSD results, significant grain refinement occurs. Despite the absence of plastic deformation the presence of nano-crystalline microstructure is observed in the steel side of the interface. This is attributed to prior machining operations performed on the substrate. It is well recognised that machining results in severe grain fragmentation [31]. Figure 5(a) shows a dark contrast at the interface in the High Angle Annular Dark Field (HAADF) imaging. This contrast could arise because of the presence of oxides at the interface. To confirm the nature of the contrast, selected area diffraction analysis was performed along the $\langle 10 \rangle$ -zone axis of the Al.

The diffraction patterns obtained from the interface clearly show the absence of oxides. The presence of ring patterns confirms the crystalline nature of the interface and the presence of fine grains. To confirm the absence of oxides energy dispersive spectroscopy shown in Figure 5(c) and (e) shows the EDS elemental maps obtained near the interface. The maps also confirm the absence of oxides at the interface between the Fe and Al. The reason for the presence of spurious Al signals in the steel interface is due the small difference in the energy of the Fe $L\alpha$ X-ray (0.705 KeV) and the Al $K\alpha$ X-ray (1.486 KeV). In addition, we also see a larger concentration of oxygen in the Fe side since some of the Fe $L\alpha$ X-rays could be indexed as an O $K\alpha$ X-ray (0.525 KeV). The EDS spectrum from the interface is shown in Figure 5(b). Note the absence of a significant oxygen peak from the interface showing the absence of oxides. Though EDS cannot quantify oxygen, it has been used extensively to detect oxygen

peaks [29,32,33]. This absence of oxides and the collapse of all the asperities at the interface confirm the original hypothesis that the enhanced bond strength of the Al-steel interface stems from the formation of a metallurgical bond. This implies that the presence of a metallurgical bond in a localised area could indeed improve the overall strength of the weld and could help in preventing a delamination type failure.

Synergy of bond formation mechanism with other solid state welding processes

To investigate whether the bonding always proceeds with the localised plastic deformation in the softer metal, the tape and substrate configurations were reversed and samples were fabricated and characterised with steel tape on an Al substrate. This was to understand the influence of configuration. For instance, while

welding a dissimilar metal combination using friction stir welding, the configuration of the material placed in the advancing side and the retreating side of the tool plays a major role [3,4]. However, this aspect of selecting the material as a tape and substrate has been overlooked in UAM.

The results from the characterisation is shown in Figure 6(a) and (c). Figure 6(a) shows the grain structure of the Al-6061 substrate. Note the presence of elongated grains that are close to 300 μm in length. Figure 6(b) shows the inverse pole figure of the interface and Figure 6(c) shows the phase map. The extent of grain refinement at the interface is clear and in this case also it is only concentrated in the Al side and not in the steel side. Further additions of steel layers were not feasible due to the high hardness of the steel and the associated nuggeting of the steel to the sonotrode horn.

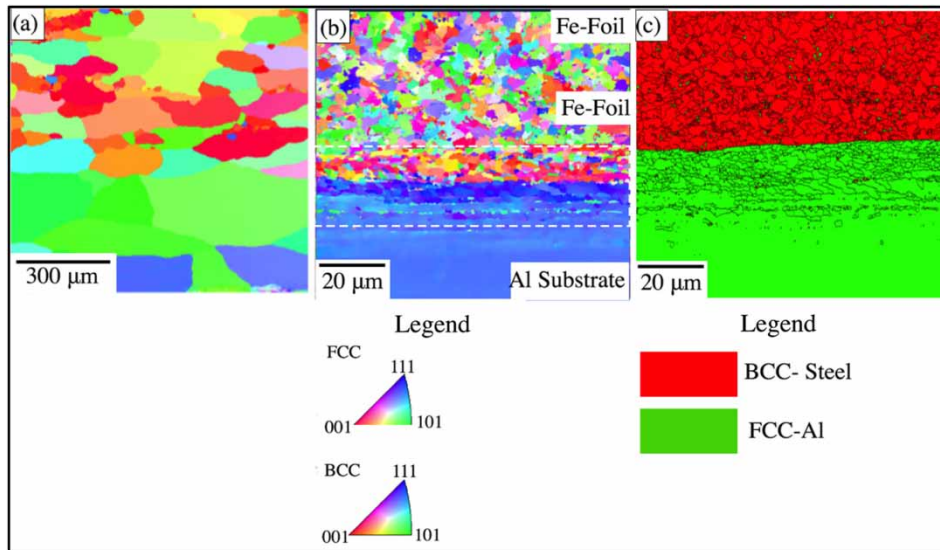


Figure 6. (a) Inverse pole figure map of the Al-6061 substrate. Note the grain sizes; (b) inverse pole figure map showing the interface. Note the refinement of grains in the Al interface; (c) grain boundary positions overlaid on a phase map where green represents Al-6061 substrate and the red represents the steel foil.

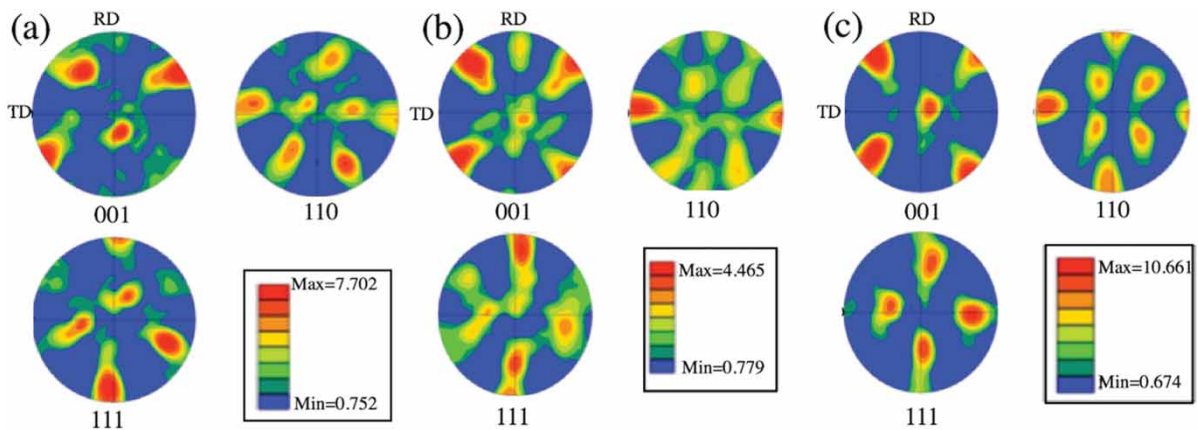


Figure 7. (a) Pole figure for the Al foil on the steel substrate. Interface showing the rotated cube component with $\{100\}$ ||normal direction and the $\langle 110 \rangle$ parallel to the direction of vibration of the sonotrode; (b) pole figure for the Al-Al interface; (c) pole figure for the Al (S)-steel (F) interface. All pole figures show the rotated cube texture at the interface.

Owing to deformation concentrating on Al, surface texture analysis of Al was performed. The {001}, {110} and {111} pole figures of the Al interfaces are presented in Figure 7(a) and (c). The pole figures show that the {110} direction is aligned with the direction of vibration of the sonotrode and the {001} pole is aligned with the normal direction. This is the rotated cube texture which is the dominant texture component observed in all the interfaces characterised. This is the texture that occurs during accumulative roll bonding [34] and also during UAM of Al-1100 and CP-Ti [18].

This similarity in texture across a wide range of material combinations explored is surprising since different process parameters were used to fabricate the Al to Al welds and the Al to steel welds. This would lead to a difference in the extent of adiabatic heating in Al when welded with steel and when welded to itself. This differential heating would change the recrystallisation behaviour, thereby changing the observed texture [35,36].

The adiabatic temperature rise in a material subject to high strain rate deformation can be calculated by integrating the dynamic flow stress over the strain range.

$$\Delta T = \frac{0.9}{\rho C_p} \int_0^{\epsilon_f} \sigma d\epsilon \quad (1)$$

The flow stress can be obtained based on constitutive equations based on dislocation dynamics as shown in Equation (2).

$$\sigma = C_0 + C_2 \epsilon' n \exp(-C_3 T + C_4 T \ln \epsilon) \quad (2)$$

The constitutive equation used is based on the Zerilli Armstrong equation [37]. C_0 , C_2 , C_3 and C_4 are constants and can be obtained from Xu et al. [14,38], ϵ' is the strain rate and ϵ is the strain. The shear strain at the interface can be estimated using the procedure described by Schick et al. [12] T is the instantaneous temperature, with exact temperatures obtained by solving Equations (1) and (2) iteratively.

Calculations show that despite the significant difference in the process parameters, the difference in adiabatic heating in Al when welded with steel is approximately 100 K. When welded with steel, the temperature rise in Al exceeds recrystallisation temperature unlike when welded to itself. However, it is surprising that the micro texture at the interface in both cases is very similar despite the difference in temperature. This may point to the insignificant role of the adiabatic heating. Bond formation in other solid state welds such as accumulative roll bonding and cold roll bonding of metals relies on plastic deformation, which serves to remove oxides and collapsing asperities. The fact that only deformation texture components are obtained in Al after UAM shows that like accumulative roll bonding, the bond formation relies on plastic deformation. This suggests that

the bonding mechanisms for both similar and dissimilar metals are the same.

Summary and conclusions

Steel and Al have been successfully fabricated using UAM. Builds were fabricated using steel as both a substrate and a foil. Mechanical testing shows a transition in the failure mode from delamination to a ductile failure. This transition results in increased strength levels of the dissimilar metal joint compared to the similar joint. Multi-scale characterisation showed that this transition in failure mode is due to the presence of localised metallurgical bonding at the interface showing that it is possible to achieve bonds with high strengths with localised regions forming a metallurgical bond. Swapping the foil and substrate configurations did not change the microstructure and texture at the interface. The observed texture is identical to the texture observed during UAM of Al and CP Ti. This suggests that similar mechanisms could operate across all dissimilar metal joints irrespective of the material combinations involved.

Acknowledgements

The authors would also like to thank Mark Norfolk of Fab-risonic LLC for providing technical support. The authors also gratefully acknowledge the US Department of Energy Advanced Manufacturing office and Dr Aslan Miriyev, Post-doctoral research scientist, Columbia University, New York for insightful discussions.

Disclosure statement

No potential conflict of interest was reported by the authors.

Funding

The authors would like to thank the Israeli Ministry of Defense (IMOD) for providing financial support for this work under contract number 1000309377.

ORCID

Sudarsanam Suresh Babu  <http://orcid.org/0000-0002-3531-2579>

References

- [1] Prangnell P, Haddadi F, Chen YC. Ultrasonic spot welding of aluminium to steel for automotive applications – microstructure and optimisation. *Mater Sci Technol*. 2011;27(3):617–624.
- [2] Taban E, Gould JE, Lippold JC. Dissimilar friction welding of 6061-T6 aluminum and AISI 1018 steel: properties and microstructural characterization. *Mater Des* (1980–2015). 2010;31(5):2305–2311.
- [3] Nandan R, DebRoy T, Bhadeshia H. Recent advances in friction-stir welding – process, weldment structure and properties. *Prog Mater Sci*. 2008;53(6):980–1023.
- [4] DebRoy T, Bhadeshia HKDH. Friction stir welding of dissimilar alloys – a perspective. *Sci Technol Weld Join*. 2010;15(4):266–270.
- [5] Choi D-H, Lee C-Y, Ahn B-W, et al. Effect of fixed location variation in friction stir welding of steels

- with different carbon contents. *Sci Technol Weld Join.* **2010**;15(4):299–304.
- [6] Watanabe T, Takayama H, Yanagisawa A. Joining of aluminum alloy to steel by friction stir welding. *J Mater Process Technol.* **2006**;178(1):342–349.
 - [7] Lee W-B, Schmucker M, Mercardo UA, et al. Interfacial reaction in steel–aluminum joints made by friction stir welding. *Scr Mater.* **2006**;55(4):355–358.
 - [8] Zhang Y. Investigation of magnetic pulse welding on lap joint of similar and dissimilar materials. Columbus (OH): The Ohio State University; **2010**.
 - [9] Zhang Y, Babu SS, Prothe C, et al. Application of high velocity impact welding at varied different length scales. *J Mater Process Technol.* **2011**;211(5):944–952.
 - [10] Mousavi AA, Al-Hassani S. Numerical and experimental studies of the mechanism of the wavy interface formations in explosive/impact welding. *J Mech Phys Solids.* **2005**;53(11):2501–2528.
 - [11] Dehoff R, Babu S. Characterization of interfacial microstructures in 3003 aluminum alloy blocks fabricated by ultrasonic additive manufacturing. *Acta Mater.* **2010**;58(13):4305–4315.
 - [12] Schick D, Hahnlen R, Dehoff R, et al. Microstructural characterization of bonding interfaces in Aluminum 3003 blocks fabricated by ultrasonic additive manufacturing. *Weld J.* **2010**;89(5):105S.
 - [13] Fujii HT, Sriraman M, Babu S. Quantitative evaluation of bulk and interface microstructures in Al-3003 alloy builds made by very high power ultrasonic additive manufacturing. *Metallur Mater Trans A.* **2011**;42(13):4045–4055.
 - [14] Xu Y, Zhang J, Bai Y, et al. Shear localization in dynamic deformation: microstructural evolution. *Metallur Mater Trans A.* **2008**;39(4):811–843.
 - [15] Bourell D, Stucker B, Obielodan J, et al. Multi material bonding in ultrasonic consolidation. *Rapid Prototyping J.* **2010**;16(3):180–188, ‘Guest editorial’.
 - [16] Obielodan J, Stucker B, Martinez E, et al. Optimization of the shear strengths of ultrasonically consolidated Ti/Al 3003 dual-material structures. *J Mater Process Technol.* **2011**;211(6):988–995.
 - [17] Truog AG. Bond improvement of Al/Cu joints created by very high power ultrasonic additive manufacturing. Columbus (OH): The Ohio State University; **2012**.
 - [18] Sridharan N, Wolcott P, Dapino M, et al. Microstructure and texture evolution in aluminum and commercially pure titanium dissimilar welds fabricated using ultrasonic additive manufacturing. *Scr Mater.* **2016**;117: 1–5.
 - [19] Wolcott P, Sridharan N, Babu S, et al. Characterisation of Al-Ti dissimilar material joints fabricated using ultrasonic additive manufacturing. *Sci Technol Weld Join.* **2016**;21(2):114–123.
 - [20] Kong C, Soar R, Dickens P. Characterisation of aluminium alloy 6061 for the ultrasonic consolidation process. *Mater Sci Eng A.* **2003**;363(1):99–106.
 - [21] Kong C, Soar R, Dickens P. Optimum process parameters for ultrasonic consolidation of 3003 aluminium. *J Mater Process Technol.* **2004**;146(2):181–187.
 - [22] Danesh Manesh H, Karimi Taheri A. Study of mechanisms of cold roll welding of aluminium alloy to steel strip. *Mater Sci Technol.* **2004**;20(8):1064–1068.
 - [23] Milner D, Rowe G. Fundamentals of solid-phase welding. *Metallur Rev.* **1962**;7(1):433–480.
 - [24] Wolcott PJ, Hehr A, Dapino MJ. Optimized welding parameters for Al 6061 ultrasonic additive manufactured structures. *J Mater Res.* **2014**;29:2055–2065.
 - [25] Zhang CS, Deceuster A, Li L. A method for bond strength evaluation for laminated structures with application to ultrasonic consolidation. *J Mater Eng Perform.* **2009**;18(8):1124–1132.
 - [26] Monaghan T, Capel AJ, Christie S, et al. Solid-state additive manufacturing for metallized optical fiber integration. *Compos A: Appl Sci Manuf.* **2015**;76: 181–193.
 - [27] Ram GJ, Yang Y, Stucker B. Effect of process parameters on bond formation during ultrasonic consolidation of aluminum alloy 3003. *J Manuf Syst.* **2006**;25(3):221–238.
 - [28] Sridharan N, Norfolk M, Babu SS. Characterization of steel-Ta dissimilar metal builds made using very high power ultrasonic additive manufacturing (VHP-UAM). *Metallur Mater Trans A.* **2016**;47(5):2517–2528.
 - [29] Shimizu S, Fujii H, Sato Y, et al. Mechanism of weld formation during very-high-power ultrasonic additive manufacturing of Al alloy 6061. *Acta Mater.* **2014**;74:234–243.
 - [30] Vaidyanath L, Nicholas M, Milner D. *Br Weld J.* **1959**;6:13–28.
 - [31] Ramesh A, Melkote S, Allard L, et al. Analysis of white layers formed in hard turning of AISI 52100 steel. *Mater Sci Eng A.* **2005**;390(1):88–97.
 - [32] Rigney D. Transfer, mixing and associated chemical and mechanical processes during the sliding of ductile materials. *Wear.* **2000**;245(1):1–9.
 - [33] Rigney D, Chen L, Naylor MG, et al. Wear processes in sliding systems. *Wear.* **1984**;100(1):195–219.
 - [34] Kim HW, Kang SB, Tsuji N, et al. Deformation textures of AA8011 aluminum alloy sheets severely deformed by accumulative roll bonding. *Metallur Mater Trans A.* **2005**;36(11):3151–3163.
 - [35] Doherty R, Hughes D, Humphreys F, et al. Current issues in recrystallization: a review. *Mater Sci Eng A.* **1997**;238(2):219–274.
 - [36] Rollett A, Humphreys F, Rohrer GS, et al. Recrystallization and related annealing phenomena. Amsterdam: Elsevier; **2004**.
 - [37] Armstrong R, Arnold W, Zerilli F. Dislocation mechanics of shock-induced plasticity. *Metallur Mater Trans A.* **2007**;38(11):2605–2610.
 - [38] Xu Y, Zhong W, Chen Y, et al. Shear localization and recrystallization in dynamic deformation of 8090 Al–Li alloy. *Mater Sci Eng A.* **2001**;299(1):287–295.